PRE- AND POST-MIDNIGHT EQUATORIAL PLASMA BUBBLES

© 2025 L. N. Sidorova

Pushkov Institute of Terrestrial Magnetism, Ionosphere and Radiowave Propagation (IZMIRAN), Moscow, Troitsk, Russia

e-mail: lsid@izmiran.ru

Received April 03, 2025

Revised April 27, 2025

Accepted May 22, 2025

Abstract. The development of the equatorial plasma bubbles is considered in the latitude-altitude and local time dynamics. Based on the revealed pattern, the features of the pre- and post-midnight equatorial plasma bubbles are investigated. For this purpose, the detailed comparative analysis of the histograms of their latitudinal and LT-variations of the occurrence probability recorded at the different altitudes was carried out. The data from the AE-E (~350−475 km), ROCSAT-1 (~600 km) and ISS-b (~972−1220 km) satellites, which had the different orbital altitudes, are included. The observations were carried out during the years of the maximal and increased solar activity. It has been revealed that the maximum of the occurrence probability of the equatorial plasma bubbles detected over the equator and low latitudes at the altitudes of ~350−1200 km develops before midnight. On the other hand, the maximum of the occurrence probability of the bubbles detected in the mid-latitude region at the altitudes of ~600−1200 km develops after midnight. It is concluded that the dominance of the post-midnight equatorial plasma bubbles in the mid-latitude region is associated with the dynamics of their rise and their increase in the geometric dimensions.

Keywords: *Equatorial plasma bubbles, latitude-altitude variations of the occurrence probability, LT-variations of the occurrence probability*

DOI: 10.31857/S00167940250511e2

1. INTRODUCTION

According to the classical theory, equatorial plasma bubbles (EPB) (and equatorial spread *F* (ESF)) are formed after sunset under the influence of the plasma instability Rayleigh− Taylor (R-T), which develops at the heights of the base of the *F region*. The development of the R-T instability is a necessary but not sufficient condition. For the beginning of generation, the presence of "seeding" plasma perturbations (seeding plasma perturbation) is also required. After sunset, i.e., with the development of the evening burst of the **E**× B drift velocity (pre-reversal enhancement, PRE), the

seed perturbations begin to evolve and form into plasma bubbles. The first EPBs appear immediately after sunset, i.e., after~ 18:00 LT. Then there is a gradual increase in the generation processes and then after~ 19:00 LT their powerful burst is observed. It has been revealed that the most intensive EPB generation at the base heights of the F-region occurs at the interval 20:00-22:00 LT [Kil and Heelis, 1998; Stolle et al., 2006].

The above scenario of EPB (ESF) development depending on local time (LT) reflects the most generally accepted point of view. Most often EPBs are observed in the pre-midnight sector and are well described within this mechanism. However, there are known cases of EPWs, the appearance of which is difficult to explain within the framework of the traditional generation theory. These are the after midnight EPWs (ESF). They were detected at the early days of research [Bowman, 1978; Burke, 1979]. However, they have been most frequently reported in recent decades [Singh et al., 1997; Kil and Heelis, 1998; Fejer et al., 1999; Palmroth et al., 2000; Yizengaw et al., 2013; Smith and Heelis, 2017; Sidorova, 2020]. Most often, these ESF cases are detected alongside ESF observations in the evening (pre-midnight) sector (AE-E (1979– 1980) [Kil and Heelis, 1998], DE 2 (1981– 1983) [Palmroth et al., 2000], and ISS-b (1978– 1979) [Sidorova, 2020]). However, EPBs detected exclusively after midnight (pre-midnight EPBs are absent) are particularly surprising. For example, they were detected from the data of radar measurements at Jikamarca station [Fejer et al., 1999]. A significant array of such EPBs was detected using data from the C/NOFS satellite for the six-year observation period (2009− 2014) covering the years of minimum and increased solar activity [Yizengaw et al., 2013; Smith and Heelis, 2017].

Attempts have been repeatedly made to explain the nature of the postmidnight ESFs. According to [Fejer et al., 1999], the generation of postmidnight ESFs is associated with anomalous reversal of the regular (usual) descending nighttime plasma drift to the ascending one. The authors believe that this reversal occurs during the period of geomagnetic perturbations, when perturbed electric fields of easterly orientation develop. These include prompt or direct penetration (PP) fields, as well as fields induced by the influence of the ionospheric disturbance dynamo (IDD). The perturbed drift raises the *F-region* to higher altitudes, where the frequency of ion-neutral collisions decreases and the growth rate of the R-T instability increases, leading to the generation of ERVs. The authors, based on long-term observations at Jikamarka station (1968− 1992), indicate that post-midnight EPWs will be more frequent in solar minimum years, since the perturbed drift in these years can easily overcome the small downward regular nighttime drifts of the quiet period. These conclusions are consistent with the results obtained from C/NOFS satellite observations (2009− 2014) [Yizengaw et al., 2013; Smith and Heelis, 2017], according to which the probability of observing post-midnight EPWs decreases as solar activity increases.

However, there is another point of view on the causes of generation of the postmidnight ESFs. According to model calculations [Su et al., 2011] based on C/NOFS, CHAMP and DMSP data, the eastward electric fields leading to the growth of the nighttime upward drift (and the subsequent generation of ESF) can appear after midnight both under the influence of geomagnetic disturbances and without them. The influence of the *E-region* dynamo, namely, the influence of the neutral wind modulated by non-migrating atmospheric tides, is pointed out as the cause of the appearance of the perturbed fields [Su et al., 2011]. This idea is supported by the results of Dao et al. [2011], according to which the longitudinal distribution of nocturnal EPWs (C/NOFS data) correlates with variations of the daytime meridional wind modulated by tidal waves calculated by the GSWM (Global Scale Wave Model).

Thus, some researchers point to the "influence from above" (geomagnetic disturbances) as the reason for the generation of postmidnight ESFs [Fejer et al., 1999]. Others claim a possible "influence from below" (atmospheric tidal waves). In the absence of a consensus, new studies and new observations covering a wider range of helio- and geophysical conditions are needed to shed light on the existing questions.

Not so long ago, in our work [Sidorova, 2020], a pronounced shift of the local ERV registration time was revealed. We considered LT-variations of the ERV observation probability calculated from data from satellites with different orbital altitudes: CHAMP (~380– 450 km), AE-E (~350– 475 km), ROCSAT-1 (~600 km), Hinotori (~650 km), and ISS- b (~972-1220 km). The analysis was performed on the ERV data sets identified over the years of satellite operation during periods of high and maximum solar activity. It was found that at the base altitudes *of the F-region* (CHAMP, AE-E), the maximum probability occurs in the post-sunset hours (~20:30– 22:00 LT); as the observation altitude increases (~600 km, ROCSAT-1), it shifts to the pre-midnight hours (~21:00– 24:00 LT), higher (~650 km, Hinotori)– to the post-midnight hours (~01:00– 03:00 LT) and finally, at upper ionospheric altitudes (~972-1220 km, ISS-b) to the predawn hours (~03:00– 04:00 LT). In other words, it is revealed that with increasing observation altitude, there is a shift of the maximum of the ERV observation probability from the pre-midnight sector to the post-midnight sector. Moreover, at the upper ionospheric heights, the overwhelming number of cases of postmidnight EPWs is detected. It turns out that one more factor associated with the increase of the probability of ERW observation in the postmidnight sector is revealed– height of observations (!).

And is it so? After all, it is well known that when the bubble rises to the upper ionosphere heights, it significantly grows in its geometrical dimensions. To all appearances, the detected altitude dependence of the LT-variation is somehow related to the geometry of the bubble. And, if so, it seems likely that the post-midnight ERVs recorded at upper ionospheric heights [Yizengaw et al., 2013; Smith and Heelis, 2017; Sidorova, 2020] experience significant latitudinal variability as well.

Moreover, there are indications for this. For example, Li et al. [2009] report a shift of the LT-interval of ERV registration to later times with increasing latitude of observation. (The observations were made during years of high and maximum solar activity (2001− 2004, *F10*.7~130-190) at ground-based sounding stations located in Southeast Asia).)

The above hypotheses are put to the test in the present study. Namely, we set the task to reconstruct the spatial and temporal pattern of EPW development from the available satellite data and investigate the features of observing pre-midnight and post-midnight EPWs. If earlier it was revealed that the probability of registration of postmidnight EPWs increases with increasing observation altitude [Sidorova, 2020], now their development will be considered in latitudinal-altitude and temporal dynamics as well. There is no doubt that this reconstruction of the EPW dynamics will allow us to approach the clarification of the problems described above.

To fulfill this task, a detailed comparative analysis of histograms of latitudinal and LT-distributions of the probability of EPB observations recorded at different altitudes was carried out. For this purpose, data from ISS-b, ROCSAT-1, and AE-E satellites with different orbital altitudes were used. Observations on these satellites were carried out in the years of maximum and increased solar activity level.

2. OBSERVATIONAL DATA

2.1 ISS-b data

EPB occurrence probability histograms (EPB occurrence probability, P_{EPB}) as a function of latitude and local time (LT) were calculated from ISS-b satellite data [RRL, 1983; 1985] (Table 1). The ISS-b satellite flew during years of high solar activity (*F10*.7~150-220, 1978-1979), had a quasi-circular orbit with an inclination of ~70° , covering the heights of the upper ionosphere (~972− 1220 km). Observations aboard the satellite were carried out for 17 months (August 1978− December 1979).

Table 1.

To calculate the histograms, observations of plasma regions with reduced He^+ concentration were used. According to [Sidorova and Filippov, 2012; Sidorova and Filippov, 2013], these regions registered at upper ionospheric heights can be interpreted as plasma bubbles of equatorial origin (EPBs). Only those EPBs (regions with depleted He^+ concentration) whose concentration decreased by a factor of one and a half or more with respect to the background were used for plotting.

To construct latitudinal variations of P_{EPB}, the data obtained for the entire observation period (August 1978− December 1979) were used. The EPB cases were considered independently of the level of geomagnetic activity in the interval 17-08 LT. The P_{EPB} values were plotted along the dipole latitudes of the Northern and Southern Hemispheres with a step of 5° in the latitudinal interval ± 60°

DIPLAT (Table 2). The obtained latitudinal variations of P_{EPB} are summarized in Fig. *1a*. The values of $P_{EPB,}$detected at equatorial and low latitudes are highlighted in dark, and at mid-latitudes– in lighter color. A schematic representation of the highlighted magnetic force tube is shown in the same figure. It is shown as an arc plotted relative to altitudes and dipole latitudes.

Fig. 1.

Table 2.

The data obtained again for the entire observation period onboard the ISS-b satellite (1978-1979) were used to construct the LT-variations of P_{EPW}. The EPW cases were considered independently of the level of geomagnetic activity in the 17-08 LT interval. The P_{EPW} values were calculated as median values for two latitudinal regions covering both hemispheres. The equatorial and low-latitude region ±20° (Fig. *2a,* left panel) was considered, as well as the predominantly mid-latitude region ± (20° -52°) (Fig. *2a,* right panel), which overlapped the low latitudes in the interval ± (20-23.3°). (The accuracy of fixing the orbital parameters of the ISS-b satellite given in the catalogs [RRL, 1983; 1985] is low, so the ±20° boundary is rather tentative. Hereafter, for ease of narration, we will refer to this region as the "mid-latitude" region). The variations of P_{ERV} obtained in the equatorial-low-latitude and mid-latitude regions are represented by dark and light colors, respectively (Fig. 2a*,* right and left panels). The numerical characteristics of the LT variations of P_{EPB} detected at different latitudes are presented in Table 3.

Fig. 2.

Table 3.

2.2 ROCSAT-1 satellite data

The ROCSAT-1 satellite was launched in 1999. It had a quasi-circular orbit with an inclination of ~35° at an altitude of ~600 km (Table 1). For the current study, we used latitude and LT-variance calculations of the probability of observing ERVs derived from the satellite data in [Su et al., 2006]. EPWs were considered as ionospheric inhomogeneities detected by ion density (*Ni*) fluctuations with a value of $\sigma > 0.3\%$. The measuring instruments used on board the ROCSAT-1 satellite had a high spatial resolution, which allowed recording inhomogeneities ranging in size from 7.5 to 75 km. EPB data detected over five years of observations (1999– 2004) covering periods of increased and maximum solar activity (*F10*.7~107– 181) were used for the calculation (Table 1).

In [Su et al., 2006], latitudinal variations of $P_{\sigma> 0.3\%}$ were plotted separately for each season. In our study, they were averaged over the entire observation period (1999– 2004). Median $P_{\sigma> 0.3\%}$ values were plotted along the dipole latitudes of the Northern and Southern Hemispheres in 5° increments over the latitudinal interval ± 55° DIPLAT (Fig. *1b*). *P* values $_{\sigma> 0.3\%}$, detected at equatorial and low

latitudes, are highlighted in darker shading, and at mid-latitudes– in lighter shading.

The data for the entire observation period (1999– 2004) were also used to construct LT variations $P_{\sigma > 0.3\%}$. The ERV cases were considered independently of the level of geomagnetic activity in the 18-09 LT interval. The data were considered in two latitude intervals: ± 30° DIPLAT (equatorial-low latitude) and ± (30°– 55°) DIPLAT (mid-latitude). $P_{\sigma > 0.3\%}$ values were plotted in one hour increments and are shown in Fig. *2b*. The histogram obtained in the equatorial-low-latitude region is presented in the left panel with a dark tone. The histogram obtained in the mid-latitude region is presented in the right panel in a lighter tone.

2.3. AE-E satellite data

For comparative analysis, data from the AE-E satellite detected during the period of high and maximum solar activity (*F10*.7~150-240, 1978-1980) were used. By this period, the satellite orbit had become nearly circular with an inclination of ~ 19.7° and covered altitudes of ~300– 475 km (Table 1). The latitude and LT variations of the EPB observation probability obtained in [Kil and Heelis, 1998] from AE-E data were used for the analysis. EPB occurrences were identified by ion density (*Ni*) fluctuations. Only those *Ni* values whose normalized index value (σ) exceeded 1% were used for calculation. (Recall that $\sigma = \Delta Ni/\bar{N}$ i, where $N\,\bar{\imath}$– is the mean value of the background ion density, andΔ *Ni*– is the standard deviation of the background ion density.) The instrument characteristics and data sampling technique used in this work allowed us to detect inhomogeneities ranging in size from 100 to .1000 км

The latitudinal variations of the EPB observation probability ($P_{\sigma > 1\%}$) obtained in [Kil and Heelis, 1998] were plotted separately for each season. In our study, they were averaged over the entire observation period (1978– 1980). The latitudinal variations of $P_{\sigma > 1\%}$ were plotted along magnetic latitudes (MLAT). Similar variations calculated from ISS-b and ROCSAT-1 satellite data were plotted along dipole latitudes (DIPLAT). And since the geomagnetic and dipole coordinates practically coincide, we will consider all latitudinal characteristics of the EPO selected for comparison along the labels of a single scale, e.g., the dipole scale (Fig. *1a*, *b, c*).

So, median $P_{\sigma > 1\%}$ values were plotted along the dipole latitudes of the Northern and Southern Hemispheres in 5° increments over the± 40° DIPLAT latitude interval (Fig. *1c*). (The authors restricted themselves to this interval because no cases of ERV outside this interval were detected.) $P_{\sigma > 0.3\%}$ values, detected at these latitudes, are highlighted in dark shading.

The figures (Fig. 1a*, b, c*) show a schematic representation of the highlighted magnetic force tube. It is shown as an arc plotted relative to the dipole latitude.

LT variations of $P_{\sigma > 1\%}$ were plotted in 30 min increments over the 19-04 LT interval. EPB cases recorded at altitudes near the maximum of the *F2* layer (~350– 475 km) in the latitude ± 40°

MLAT interval were used to calculate $P_{\sigma>1\%}$. Median $P_{\sigma>1\%}$ values, calculated over two years of observations (1978– 1980), are shown in Fig. *2c* in dark.

3. COMPARATIVE ANALYSIS

1. Let us perform a detailed comparative analysis of the latitudinal variations of the EPB observation probability revealed by the ISS-b, ROCSAT-1, and AE-E satellite data (Fig. *1a*, *b, c*).

According to observations obtained on board the AE-E satellite, at altitudes near the maximum of the *F2* layer (~350– 475 km), ERVs are registered in a rather wide interval± 40° DIPLAT. The latitudinal histogram $P_{\sigma>1\%}$ has the shape of a Gaussian normal distribution. The bulk of ERVs are recorded over the equator and at low latitudes within ± 25° DIPLAT, and a small number of ERV occurrences fall within the "tails" of the± (25°– 35°) distribution (Fig. *1c*). The maximum $P_{\sigma>1\%}$, developing over the equator, reaches a value of~ 40%.

At altitudes of ~600 km (ROCSAT-1), the latitudinal distribution of the EPB observation probability ($P_{\sigma>0.3\%}$) begins to change dramatically (Fig. *1b*). In the latitudinal variations of $P_{\sigma>0.3\%}$, additional mid-latitude maxima develop in addition to the central (equatorial) maximum of the probability. These occur at latitudes ~(± 50°) DIPLAT. The magnitudes of the central maximum and the Southern Hemisphere midlatitude maximum are comparable (~9%). The Northern Hemisphere midlatitude maximum is slightly less developed– ~3%. The central (equatorial) maximum becomes narrower (in the interval ± 20° DIPLAT) compared to the similar maximum from the AE-E satellite data (Fig. *1c*).

At the upper ionospheric heights (~972-1220 km, ISS-b), the mid-latitude maxima of P_{EPW} become more pronounced and begin to dominate over the central (equatorial) maximum (Fig. *1a*). Their magnitudes are ~17% and ~11% in the Southern and Northern Hemispheres, respectively. The magnitude of the central maximum P_{EPB} is slightly inferior to them– ~ 9%. The midlatitude maxima appear no longer at the former latitudes (~± 50° DIPLAT), but at latitudes (~± 45°) DIPLAT, slightly shifted to the equator (Fig. *1a*, *b*). (The reasons for this shift will be discussed in the next section.) The central (equatorial) maximum remains as narrow (in the interval ± 20° DIPLAT).

It should be noted that we do not compare the latitudinal probability distributions of EPB observations plotted at different altitudes with each other in terms of absolute values. We believe that such a comparison is incorrect, since the above distributions were calculated from observations of different satellites with measuring instruments of different types. And different approaches and methods of data processing were used to identify EPB structures.

2. Let us now turn to the LT-variations of the EPB observation probability detected from ISS-

b, ROCSAT-1, and AE-E data at different altitudes (Fig. *2a*, *b, c*).

Since EPBs detected at different altitudes showed such a striking latitudinal variability, it is reasonable to consider the LT-variations of the EPB observation probability by individual latitudinal regions. As was revealed earlier (Fig. *1a*, *b, c*), ERVs with increasing observation altitude begin to split into two groups– the group forming the central (equatorial) maximum and the group of ERVs forming midlatitude maxima. For this reason, LT variations were obtained at each altitude for the latitudinal group forming the central (equatorial) maximum (left panel in Fig. *2a*, *b, c*) and the EPB group forming the midlatitude maxima (right panel in Fig. *2a*, *b*). We consider the latter group as a single group regardless of the fact that the ERV cases were recorded in different hemispheres. The latitude intervals of these groups, as shown above, vary slightly with increasing observational height.

Let us first consider the LT-variations of the probability of EPB observations near the central latitudinal maximum.

As indicated above, LT variations of $P_{\sigma>1\%}$ were plotted for the± 40° DIPLAT interval centered relative to the equator using data from the AE-E satellite (~350– 475 km) (Fig. *2c,* left panel). It is well observed that the first ERVs appear just after sunset, i.e., after~ 18:00 LT. The maximum $P_{\sigma>1\%}$ (~24-25%) is reached by ~21:00 LT and holds for almost 2 hours until ~23:00 LT. Thereafter, there is a fairly gradual drop in $P_{\sigma>1\%}$ values until ~7:00 AM LT.

A similar pattern develops in the LT variations of $P_{\sigma>0.3\%}$, detected from ROCSAT-1 satellite data (~600 km) in the± 30° DIPLAT interval (Fig. 2b*,* left panel). It can be seen that the first ERVs appear after sunset (~ 19:00 LT). The maximum $P_{\sigma>0.3\%}$ (~13%) is reached by~ 20:00– 22:00 LT. However, after ~22:00 LT, the $P_{\sigma>1\%}$ values of begin to decline smoothly. A drop in $P_{\sigma>1\%}$ values develops in the post-midnight sector as well, and they finally fade away by the morning hours (~7:00 LT).

If we consider the LT variations of P_{EPB} obtained from the ISS-b satellite data (~972-1220 km) in the interval± 20° DIPLAT (Fig. *2a,* left panel), we notice that the picture is somewhat distorted. As before, the development of the P_{EPB} maximum (~40– 42%) is reached by ~21:00– 23:00 LT. However, there is then a sharp drop in P_{EPB} values after ~23:00 LT. The reduced P_{EPB}values remain at approximately the same rather high level (~30%) for an extended period of time (until~ 5:00 LT). After~ 5:00 LT, there is another sharp drop in P_{EPB}values (to ~7%) that finally fades by ~8:00 LT.

If we consider the LT variations of the probability of EPB observations in the region of mid-latitude maxima, we point out that they were calculated only from data from the ISS-b (~972-1220 km) and ROCSAT-1 (~600 km) satellites (Fig. 2a*, b,* right panels).

Using data from the ROCSAT-1 satellite, LT variations of $P_{\sigma>0.3\%}$ were plotted for the± (30°–

50°) DIPLAT intervals (Fig. *2b,* right panel). It is well seen that the first ERV cases at these latitudes are recorded already after sunset (~ 19:00 LT). Thereafter, a very smooth increase in $P_{\sigma > 0.3\%}$ values is observed all the pre-midnight time. The $P_{\sigma > 0.3\%}$ value reaches its maximum (~2– 3%) in the post-midnight sector at ~2:00 LT. Thereafter, there is a sharper decline in $P_{\sigma > 0.3\%}$ values until their complete decay in the morning at~ 8:00 LT.

Using data from the ISS-b satellite, LT variations of P_{EPB}were plotted for the interval± (20°– 52°) of DIPLAT (Fig. 2a*,* right panel). It is clearly seen that the first occurrences of EPB at these latitudes are recorded with sunset (~ 18:00 LT). Then there is a steady increase of P_{EPB}values ,reaching its maximum (~36%) well after midnight, namely closer to the predawn hours (~ 3:00– 4:00 LT). There is then a fairly sharp drop in values towards the morning hours (~ 7:00– 8:00 LT).

4. DISCUSSION

As stated in the Introduction, the aim of the present study is to construct a spatio-temporal picture of the EPW development and to investigate the observational features of pre-midnight and post-midnight EPWs. For this purpose, satellite data with different orbital altitudes were involved: ISS-b (~972-1220 km), ROCSAT-1 (~600 km), AE-E (~350– 475 km).

To achieve this goal, a latitude-altitude picture of the EPW evolution was initially constructed. The revealed picture allowed us to detect the characteristic latitudinal-altitude features of the EPW: equatorial and midlatitude maxima of the observation probability. Further, the development of these features was examined in time. This allowed us to observe the spatial and temporal dynamics of EPW in the pre-midnight sector and (of particular interest to us) in the post-midnight sector. Let us consider the above stages of the research in detail.

1) First, let us discuss the latitudinal-altitude picture of EPW development.

From the comparison of latitudinal distributions of the ERV observation probability obtained at different altitudes (AE-E, ROCSAT-1, ISS-b), it was revealed that as the observation altitude increases, in addition to the central (equatorial) maximum of the probability, mid-latitude maxima begin to develop (Fig. *1a*, *b, c*). What is happening? To explain, let us use a schematic representation of the evolution of the ERV with respect to dipole latitudes, altitude, and magnetic force tubes (Fig. *1g*).

As is known, plasma bubbles, as they rise to higher heights under the influence of ambipolar diffusion, begin to "stretch/spread" along the magnetic force tubes, acquiring a banana-shaped appearance (Fig. *1g*). At the initial phase of their development (the height of the *F-region* base), the bubbles are still registered within the equatorial region. Further, as they rise, diffusive "spreading" processes come into force and EPBs can be registered not only in equatorial, but also in low latitudes. This is evidenced by data from the AE-E satellite (~350– 475 km) (Fig. 1c*, d*). The latitudinal

distribution ($P_{\sigma>1\%}$) takes the form of a Gaussian normal distribution centered relative to the equator. The bulk of ERVs at these altitudes are recorded in the± 25° DIPLAT interval and only a small number of cases occur in the "tails" of the± distribution (25°– 35°). With further ascent, the bubbles are increasingly "stretched" along magnetic force tubes (ROCSAT-1, ~600 km). At the same time, the middle (apex) part of the rising bubble is registered above the equator, and its "ends" are projected not only to low, but also to middle latitudes (Fig. 1b*, d*). This EPB dynamics is reflected in latitude histograms $P_{\sigma>0.3\%}$: in addition to the central (equatorial) maximum of probability, additional midlatitude maxima begin to develop in the Northern and Southern Hemispheres (Fig. 1b*, d*).

Why do these additional maxima appear? After all, it is logical to expect that the rise of bubbles will be accompanied only by broadening of the central (equatorial) maximum! We suppose that the development of the latter is explained by the fact that the EPB has reached its ceiling heights. (According to theoretical studies [Ott, 1978; Ossakov and Chaturvedi, 1978], the ceiling height of a plasma bubble is determined by the condition under which the equality of the plasma concentration of the bubble and the external medium is reached). In this case, the bubbles lose the ability to rise further, experience deceleration, stop at the force tube corresponding to the ceiling height, and experience collapse (contraction) after several hours. Bubbles "frozen" at their ceiling heights accumulate, which is reflected in the appearance of midlatitude maxima of their probability of observation.

This pattern is most pronounced at upper ionospheric heights (ISS-b, ~972-1220 km) (Fig. 1a*, d*). The midlatitude maxima of $P_{EPB}$are the most pronounced here. However, they appear not at the former latitudes (~± 50°) of DIPLAT, but at latitudes (~± 45°) of DIPLAT, slightly shifted to the equator (Fig. *1a*, *b*). The reason for this lies in the latitude-altitude course of the magnetic force tubes. For illustration, the course of one of them is shown on the latitudinal distributions of the probability of ERV observations based on data from different satellites (Fig. *1a*, *b, c*).

It should be mentioned that the latitudinal-altitude behavior of the EPWs revealed by us is quite expected, since we have previously constructed similar histograms using data from ISS-b, ROCSAT-1, and AE-E satellites in separate seasons [Sidorova, 2021]. Now, pursuing somewhat different goals - the study of the features of pre-midnight and post-midnight EPWs, we obtained a latitude-altitude picture of EPW development for the full observation intervals of the mentioned satellites.

2) We now discuss the development of the identified latitude-altitude features of the EPO as a function of local time (Fig. *2a*, *b*, *c*; right and left panels).

For this purpose, LT variations of the probability of observing EPBs were obtained at different altitudes and recorded in the following latitudinal regions– in the region of (a) equatorial maxima and (b) midlatitude maxima. Moreover, EPBs detected at midlatitudes of different hemispheres were considered together.

Let us point out an important feature that was revealed during the analysis. It was obtained that ERVs after midnight can be observed both in the region of the equator and low latitudes and in the region of middle latitudes. However, depending on the latitudinal region, their LT variations have different developmental trends. Thus, the number of postmidnight ERVs recorded at the equator and low latitudes (Fig. 2a*, b, c*; left panel) steadily decreases during this period toward the morning hours. Conversely, the number of postmidnight EPWs recorded at midlatitudes (Fig. 2a*, b;* right panel) increases and reaches its maximum (ISS-b and ROCSAT-1).

We analyze the development of EPWs as a function of local time in the indicated latitude regions.

The equator and low latitudes– region of the central (equatorial) latitudinal maximum (Fig. *2a*, *b*, *c*; left panel). Recall that at these latitudes the bubbles are "visible" almost entirely from the AE-E satellite data (~350– 475 km). At ROCSAT-1 altitudes (~600 km), most of the bubbles are "visible", and at ISS-b altitudes (~972-1220 km, upper ionosphere), either the tops of the bubbles or the parts of the bubbles closest to the tops are recorded (see Fig. *1d*).

Let us point out that all LT variations calculated at different altitudes are characterized by a sharp pre-midnight probability spike. The probability maximum is reached at ~21:00– 23:00 LT from AE-E data (~350– 475 km), at ~20:00– 21:00 LT from ROCSAT-1 data (~600 km), and at ~22:00– 23:00 LT from ISS-b data (~972-1220 km). Then there is a gradual more or less smooth fading of the probability values towards the morning hours. In other words, the available satellite data (AE-E, ROCSAT-1, ISS-b) show that most ERVs develop before midnight, but there are a number of cases observed after midnight.

Let us consider a group of postmidnight EPWs in this latitudinal region and obtain numerical estimates.

There is no doubt that the post-midnight (as well as pre-midnight) data of the AE-E satellite at these latitudes are essentially a "snapshot" of the EPB generation processes, since the orbital altitudes of the satellite (~350– 475 km) are close to the base of the F-region, i.e., to the bubble generation altitudes. The plasma bubble generated at night reaches the altitudes of ~600 km (ROCSAT-1) and ~1000 km (ISS-b) somewhat later. It is possible to estimate the characteristic rise time of the top of such a bubble to a height of, for example, ~1000 km. It is known that the bubble ascent velocity varies in the range from ~150 m/s to ~1 km/s. (According to ion-probe [Abdu et al., 1983], satellite (AE-C, [McClure et al., 1977]), and radar [Woodman and La Hoz, 1976] measurements, bubble ascent velocities can be≥ 150 m/s. On the other hand, there are reports of "fast" bubbles rising at velocities on the order of ~1 km/s [Hanson et al., 1997; Huba et al., 2008]). If we calculate the bubble rise time at these extreme velocity values, it will vary from ~10 minutes to one hour. In other words, the bubbles that appeared at night will be "visible" at the upper ionosphere altitudes (~1000 km) in less than an

hour if they are considered in the region of equatorial and low latitudes. And, since the processes in this latitude-altitude region are very dynamic, there is no doubt that the EPBs registered after midnight at the altitudes of ~600 and ~1000 km are the bubbles, which appeared also quite recently, i.e., at night or already after midnight.

Midlatitudes– region of midlatitude maxima (Fig. *2a*, *b*; right panel). The picture is somewhat different in the midlatitude region. Let us point out that at these latitudes the values of LT-variations of the probability of ERV observations, calculated for altitudes of ~600 km and ~1000 km, grow smoothly before midnight, reach their maxima after midnight (at~ 02:00 LT from ROCSAT-1 data (~600 km); at~ 03:00– 04:00 LT from ISS-b data (~972-1220 km)) and fall rather sharply by the morning hours. What is happening at these latitudes?

As mentioned above, the appearance of mid-latitude maxima of the ERB observation probability indicates that the bubbles managed to reach their ceiling heights, stop there and accumulate. If we turn to the schematic image of the EPB rise (Fig. *1g*), we can clearly see that in the midlatitude region the satellites fix "tails" of plasma bubbles "stretched" along the power tubes. Moreover, the tops of such "stretched" bubbles reach very high ionospheric heights (from 2000 km and higher). (According to Burke et al. [1979] bubbles in such a state are well determined even at heights of ~3500 km.) Obviously, for a bubble to rise to such heights, it takes much longer time. It is possible to estimate the time for the top of the bubble to rise, for example, to an altitude of ~3500 km. It will vary greatly depending on the rate of ascent . For "fast" bubbles it will be ~50 min, and for ordinary– up to 5.5 hours!

It can be assumed that the fraction of "fast" bubbles is small compared to the fraction of "ordinary" (regular) bubbles, which have much lower velocities, e.g.,~ 200– 600 m/s. And, indeed, this is confirmed by the shape of the LT-variations in the pre-midnight sector (Fig. *2a*, *b*; right panel). Here, the LT-variance values increase quite smoothly. This means that at first, in the pre-midnight hours, only some "fast" bubbles manage to reach their ceiling heights, "freeze" there and accumulate. Then, more and more bubbles, which are not so "fast", join this process (Fig. *2a*, *b*; right panel, pre-midnight hours). Then, in the post-midnight hours, the maximum probability of ERB observation rapidly develops (Fig. *2a*, *b*; right panel, post-midnight hours). This occurs because already the main mass of bubbles, consisting of "ordinary" bubbles, after several hours manages to reach these heights and "freeze" there. And when comparing the left and right panels of Fig. 2, it is easy to see that the time gap between the appearance of maximums of the ERB observation probability in the equator/low latitude and mid-latitude regions is ~5– 6 h according to both ROCSAT-1 and ISS-b data. Obviously, the development of maxima in both latitudinal regions marks the "arrival" of the main mass of "ordinary" bubbles at these altitudes/latitudes and indicates their dominant contribution.

By morning, the values of LT-variations of the probability of ERV observation experience a rather sharp decline (Fig. *2a*, *b*; right panel). This is explained by the following. Bubbles "frozen" near their ceiling heights, getting into the morning and further into the daytime sector, are exposed to powerful photoionization processes that begin to restore the underestimated concentrations of their ionic components, which leads the bubbles to dissipation [Sidorova and Filippov, 2014].

Thus, it turns out that the dominant time of their registration changes dramatically with the change of the latitude of EPB observations. In observations over the equator/low latitudes, they are registered mainly before midnight, and in observations over midlatitudes - after midnight. And the reason for the latter is the long rise time of the plasma bubble, its dynamical characteristics, and the giant geometric size of the developed bubble (see, for example, [Comberiate and Paxton, 2010]).

However, if the appearance of EPBs at midlatitudes in the postmidnight hours can be explained by the duration of the ascent, dynamics and geometry of the bubble, the reasons for the appearance of EPBs at the equator/low latitudes after midnight still raise many questions.

As discussed in the Introduction, a number of factors have been found to favor ERV generation after midnight. Fejer et al. [1999], having studied multiyear radar data obtained at Jikamarca station (1968− 1992), pointed to the influence of geomagnetic perturbations and conditions of decreased solar activity. The results obtained in studies using C/NOFS satellite data (2009− 2014) are consistent with these conclusions [Yizengaw et al., 2013; Smith and Heelis, 2017]. Recall that these data sets were significant in terms of the observation period but limited in the observational latitudes. The C/NOFS satellite with an equatorial orbit (inclination 13°) had only the equator and the near-equatorial zone available for viewing. Radar measurements were made at latitude− 11.95° DIPLAT with a scan angle of 1° . In other words, the latitudinal coverage was at equatorial latitudes, i.e., the latitudes of EPW generation. (Ideal series for studying the generation and initial stages of EPW development!) And, it would seem, exhaustive conclusions about the possible causes of the generation of post-midnight EPWs were obtained.

However, over time, alternative views on this subject have emerged. Su et al. [2011] suggested that nocturnal and postmidnight EPWs can develop under the influence of tidal waves. In this case, the authors [Su et al., 2011] relied on the results of modeling using data from the C/NOFS, CHAMP and DMSP satellites. The modeling results obtained by another group of researchers [Dao et al., 2011], which used data from the same C/NOFS, did not contradict these conclusions. (According to the latter, the longitudinal distribution of nocturnal EPWs correlates with variations in the daytime meridional wind modulated by tidal waves).) We should also mention the results we obtained [Sidorova and Filippov, 2018; Sidorova and Filippov, 2018] using ISS-b satellite data. We showed that at upper ionospheric altitudes (ISS-b, ~972-1220 km) the longitude distribution of nighttime EPWs clearly correlates ($R\cong$ 0.69) with the longitude profile of evening deviations of the

thermospheric zonal wind speed (CHAMP, ~400 km) modulated by the DE3 tidal wave. This is further evidence in favor of the idea of Su et al. [2011].

Summarizing the above, we conclude that to date there is no consensus on the causes of the generation of postmidnight EPWs detected at the equator and at low latitudes. The nature of these EPWs is still unclear, and the ideas of their generation need additional verification.

We can speak unambiguously only about the nature of the postmidnight EPWs that are detected in the region of middle latitudes. These are bubbles that were generated during the traditional evening hours. These are bubbles "stretched" along magnetic force tubes, which allows them to be detected even at mid-latitudes. Finally, these are the bubbles that were able to reach significant heights of the upper ionosphere after ~5– 6 h and "freeze" there.

5. CONCLUSION

Studies of equatorial plasma bubbles formed under the influence of the Rayleigh-Taylor plasma instability at the base heights *of the* F-region are still relevant. In this work, the spatial and temporal picture of the EPB development is reconstructed using satellite data. Namely, the EPW development is considered in latitudinal-altitude and temporal dynamics. According to the revealed picture, the peculiarities of observation of pre-midnight and post-midnight EPWs were investigated. For this purpose, a detailed comparative analysis of the histograms of latitudinal and LT-distributions of the probability of EPB observations recorded at different altitudes was carried out. Data from AE-E (~350– 475 km), ROCSAT-1 (~600 km), and ISS-b (~972-1220 km) satellites with different orbital altitudes were involved. The observations were carried out in the years of maximum and increased solar activity. The following conclusions are drawn as a result of the study.

1. The maximum probability of observing ERVs detected in the equatorial and low latitude regions at altitudes of ~350-1200 km develops before midnight.

2. The maximum of the probability of observation of EPWs detected in the region of middle latitudes at altitudes ~600-1200 km develops after midnight. The dominance of post-midnight EPWs in this latitude-altitude region is associated with the dynamics of the rise and growth of geometric sizes of plasma bubbles.

REFERENCES

1. *Sidorova L.N., Filippov S.V.* Longitude statistics of plasma "bubbles" visible at altitudes of the upper ionosphere in concentrations Not+ // Geomagnetism and aeronomy. V. 53. No. 1. P. 64-77. 2013. https://doi.org/10.7868/S0016794012060107

2. *Sidorova L.N., Filippov S.V.* Equatorial plasma “bubbles": The influence of thermospheric winds modulated by the DE3 tidal wave // Geomagnetism and Aeronomy. V. 58. No. 2. P. 225-233. 2018. https://doi.org/10.7868/S0016794018020086

3. *Sidorova L.N.* Equatorial plasma bubbles: The dependence of the probability of observation on local time // Geomagnetism and aeronomy. V. 60. No. 5. P. 557-565. 2020. https://doi.org/10.31857/S0016794020050144

4. *Sidorova L.N.* Equatorial plasma bubbles: Variability of latitude distribution with altitude // Geomagnetism and Aeronomy. V. 61. No. 4. P. 445-456. 2021. https://doi.org/10.31857/S0016794021040167

5. *Abdu M.A., de Medeiros R.T., Sobral J.H.A., Bittencourt J.A.* Spread *F* plasma bubble vertical rise velocities determined from spaced ionosonde observations // J. Geophys. Res. – Space. V. 88. № 11. P. 9197–9204. 1983. https://doi.org/10.1029/JA088iA11p09197

6. *Bowman G.G.* A relationship between polar magnetic substorms, ionospheric height rises and the occurrence of spread *F* // J. Atmos. Terr. Phys. V. 40. № 6. P. 713–722. 1978. https://doi.org/10.1016/0021-9169(78)90129-0

7. *Burke W.J.* Plasma bubbles near the dawn terminator in the topside ionosphere // Planet. Space Sci. V. 27. № 9. P. 1187−1193. 1979. https://doi.org/10.1016/0032-0633(79)90138-7

8. *Burke W.J., Donatelli D.E., Sagalyn R.C., Kelley M.C.* Low density regions observed at high altitudes and their connection with equatorial spread *F* // Planet. Space. Sci. V. 27. № 5. P. 593−601. 1979. https://doi.org/10.1016/0032-0633(79)90157-0

9. *Comberiate J., Paxton L.J.* Coordinated UV imaging of equatorial plasma bubbles using TIMED/GUVI and DMSP/SSUSI // Space Weather. V. 8. № 10. ID S10002. 2010. https://doi.org/10.1029/2009SW000546

10. *Dao E., Kelley M.C., Roddy P., Retterer J., de La Beaujardière O., Su Y.-J.* Longitudinal and seasonal dependence of nighttime equatorial plasma density irregularities during solar minimum detected on the C/NOFS satellite // Geophys. Res. Lett. V. 38. № 10. ID L10104. 2011. https://doi.org/10.1029/2011GL047046

11. *Fejer B.G., Scherliess L., de Paula E.R.* Effects of the vertical plasma drift velocity on the generation and evolution of equatorial spread *F* // J. Geophys. Res. – Space. V. 104. № 9. P. 19859–19869. 1999. https://doi.org/10.1029/1999JA900271

12. *Hanson W.B., Coley W.R., Heelis R.A., Urquhart A.L.* Fast equatorial bubbles // J. Geophys. Res. – Space. V. 102. № 2. P. 2039−2045. 1997. https://doi.org/10.1029/96JA03376

13. *Huba J.D., Joyce G., Krall J.* Three-dimensional equatorial spread *F* modeling // Geophys. Res. Lett. V. 35. № 10. ID L10102. 2008. https://doi.org/10.1029/2008GL033509

14. *Kil H., Heelis R.A.* Global distribution of density irregularities in the equatorial ionosphere // J. Geophys. Res. – Space. V. 103. № 1. P. 407−417. 1998. https://doi.org/10.1029/97JA02698
15. *Li G., Ning B., Liu L., Wan W., Liu J.Y.* Effect of magnetic activity on plasma bubbles over equatorial and low-latitude regions in East Asia // Ann. Geophys. V. 27. № 1. P. 303–312. 2009. https://doi.org/10.5194/angeo-27-303-2009
16. *McClure J.P., Hanson W.B., Hoffman J.F.* Plasma bubbles and irregularities in the equatorial ionosphere // J. Geophys. Res. V. 82. № 19. P. 2650−2656. 1977. https://doi.org/10.1029/JA082i019p02650
17. *Ott E.* Theory of Rayleigh−Taylor bubbles in the equatorial ionosphere // J. Geophys. Res. – Space. V. 83. № 5. P. 2066−2070. 1978. https://doi.org/10.1029/JA083iA05p02066
18. *Ossakov S.L., Chaturvedi P.K.* Morphological studies of rising equatorial spread *F* bubbles // J. Geophys. Res. – Space. V. 83. № 5. P. 2085−2090. 1978. https://doi.org/10.1029/JA083iA05p02085
19. *Palmroth M., Laakso H., Fejer B.G., Pfaff R.F. Jr.* DE 2 observations of morningside and eveningside plasma density depletions in the equatorial ionosphere // J. Geophys. Res. – Space. V. 105. № 8. P. 18429–18442. 2000. https://doi.org/10.1029/1999JA005090
20. *RRL.* Summary plots of ionospheric parameters obtained from Ionosphere Sounding Satellite-b. Tokyo: Radio Research Laboratories. Ministry of Posts and Telecommunications. V. 1−3. 1983.
21. *RRL.* Summary plots of ionospheric parameters obtained from Ionosphere Sounding Satellite-b. Tokyo: Radio Research Laboratories. Ministry of Posts and Telecommunications. Special Report. V. 4. 1985.
22. *Sidorova L.N., Filippov S.V.* Topside ionosphere He^+ density depletions: seasonal/longitudinal occurrence probability // J. Atmos. Sol.-Terr. Phy. V. 86. P. 83–91. 2012. https://doi.org/10.1016/j.jastp.2012.06.013
23. *Sidorova L.N., Filippov S.V.* Plasma bubbles in the topside ionosphere: estimations of the survival possibilities // J. Atmos. Sol.-Terr. Phy. V. 119. P. 35–41. 2014. https://doi:10.1016/j.jastp.2014.06.013
24. *Sidorova L.N., Filippov S.V.* Four-peak longitudinal distribution of the equatorial plasma bubbles observed in the topside ionosphere: Possible troposphere tide influence // Adv. Space Res. V. 61. № 6. P. 1412–1424. 2018. https://doi.org/10.1016/j.asr.2017.12.035
25. *Singh S., Bamgboye D.K., McClure J.P., Johnson F.S.* Morphology of equatorial plasma bubbles // J. Geophys. Res. – Space. V. 102. № 9. P. 20019−20029. 1997. https://doi.org/10.1029/97JA01724
26. *Smith J., Heelis R.A.* Equatorial plasma bubbles: Variations of occurrence and spatial scale in local time, longitude, season, and solar activity // J. Geophys. Res. – Space. V. 122. № 5. P.

5743−5755. 2017. https://doi: 10.1002/2017JA024128
27. *Stolle C., Lühr H., Rother M., Balasis G.* Magnetic signatures of equatorial spread *F* as observed by the CHAMP satellite // J. Geophys. Res. – Space. V. 111. № 2. ID A02304. 2006. https://doi.org/10.1029/2005JA011184
28. *Su S.-Y., Liu C.H., Ho H.H., Chao C.K.* Distribution characteristics of topside ionospheric density irregularities: Equatorial versus midlatitude regions // J. Geophys. Res. – Space. V. 111. № 6. ID A06305. 2006. https://doi: 10.1029/2005JA011330
29. *Su Y.-J., Retterer J.M., Pfaff R.F., Roddy P.A., de La Beaujardière O., Ballenthin J.O.* Assimilative modeling of observed postmidnight equatorial plasma depletions in June 2008 // J. Geophys. Res. – Space. V. 116. № 9. ID A09318. 2011. https://doi.org/10.1029/2011JA016772
30. *Woodman R.F., La Hoz C.* Radar observations of *F*-region equatorial irregularities // J. Geophys. Res. V. 81. № 31. P. 5447−5466. 1976. https://doi.org/10.1029/JA081i031p05447
31. *Yizengaw E., Retterer J., Pacheco E.E., Roddy P., Groves K., Caton R., Baki P.* Postmidnight bubbles and scintillations in the quiet-time June solstice // Geophys. Res. Let. V. 40. № 21. P. 5592−5597. 2013. https://doi:10.1002/2013GL058307

Table 1. Data used in the comparative analysis

Publication	Satellite	Para-meter	LT-interval	Altitudes, km	Latitudes	Years	$F10.7$
Our study	ISS-b	P_{EPB}	17:00– 08:00	~972-1220	±60° DIPLAT	1978– 79	150–220
Su et al, 2006	ROCSAT-1	$P_{\sigma>0.3\%}$	18:00– 09:00	~600	±30° DIPLAT;	1999– 04	107– 181

					±(30°– 55)° DIPLAT		
Kil and Heelis, 1998	AE-E	$P_{\sigma > 1\%}$	19:00– 04:00	~300 475–	±40° MLAT	1978– 80	150– 240

Table 2. Numerical characteristics of latitudinal variations of EPB observation probability (P_{EPB}) calculated from ISS-b data for the entire observation period (August 1978– December 1979).

Dipole latitude, deg	Number EPBs and overflights[1]	P_{EPB}[2], %
-55	61 (738)	8
-50	107 (766)	14
-45	133 (800)	17
-40	95 (813)	12
-35	63 (809)	8
-30	47 (808)	6
-25	22 (818)	3
-20	17 (818)	2
-15	28 (817)	3
-10	48 (814)	6
-5	73 (817)	9
0	75 (832)	9
5	45 (828)	6
10	41 (824)	5
15	24 (815)	3
20	11 (805)	1
25	41 (785)	5
30	49 (776)	6
35	78 (770)	10
40	80 (793)	10
45	86(764)	11
50	60 (754)	8
55	37(742)	5

Note:

[1]The ISS-b satellite had technical interruptions, which was reflected in the non-uniformity of orbital coverage by the dipole latitude parameter.

[2]P_{ERV}values are rounded to whole numbers.

Table 3. Numerical characteristics of the LT variations of the EPB observation probability ($P_{EPB)}$ calculated from the ISS-b satellite data at equator/low latitudes and at mid-latitudes

LT, h	EQUATOR/LOW LATITUDES ±20° DIPLAT		MEDIUM LATITIES ±(20° -52°) DIPLAT	
	Number ERW and spans[1]	P_{ERV}[2], %	Number Number of EPO and spans[1]	P_{ERV}[2], %
14	0 (45)	0	0 (191)	0
15	0 (49)	0	0 (240)	0
16	0 (51)	0	0 (285)	0
17	0 (63)	0	0 (310)	0
18	3 (70)	4	15 (350)	4
19	6 (74)	8	33 (385)	9
20	20 (107)	19	60 (474)	13
21	48 (124)	39	70 (502)	14
22	48 (116)	41	86 (503)	17
23	40 (96)	42	102 (521)	20
24(00)	33 (111)	30	105 (511)	21
01	28 (104)	27	135 (486)	28
02	28 (92)	30	132 (497)	27
03	26 (91)	29	144 (462)	31
04	30 (100)	30	161 (447)	36
05	23 (92)	25	108 (422)	26
06	5 (76)	7	65 (418)	16
07	3 (47)	6	22 (341)	6
08	2 (50)	4	4 (245)	2
09	0 (61)	0	0 (210)	0
10	0 (53)	0	0 (198)	0

Note:

[1]The ISS-b satellite had technical interruptions, which was reflected in the non-uniformity of orbital coverage by the LT parameter.

[2]P_{ERV}values are rounded to whole numbers.

FIGURE CAPTIONS

Fig. 1. Latitudinal variations of the EPB observation probability.
(*a*) ISS-b data for the period 1978-1979, altitudes ~972-1220 km, ±60° DIPLAT.
(*b*) ROCSAT-1 data for the period 1999-2004, altitudes ~600 km, ±55° DIPLAT.
(*c*) AE-E satellite data for the period 1979-1980, altitudes ~350– 475 km, ±40° DIPLAT.
(*d*) Schematic representation of the evolution of equatorial plasma bubbles with respect to dipole latitudes, altitudes, and magnetic force tubes. Horizontal lines show the approximate flyby altitudes of the ISS-b (~972-1220 km), ROCSAT-1 (~600 km), and AE-E (~350– 475 km) satellites.

Fig. 2. LT variations of the probability of EPB observation.
(*a*) ISS-b satellite data for the period 1978-1979, altitudes ~972-1220 km. Equator and low latitude region: ±20° DIPLAT (left panel). Mid-latitude region: ±(20°-52°) DIPLAT (right panel).
(*b*) ROCSAT-1 satellite data for the period 1999-2004, altitudes ~600 km. Equatorial and low latitude region: ±30° DIPLAT (left panel). Mid-latitude region: ±(30°-55°) DIPLAT (right panel).
(*c*) AE-E satellite data for the period 1979-1980, altitudes ~350– 475 km. Latitude region: ±40° DIPLAT (left panel).

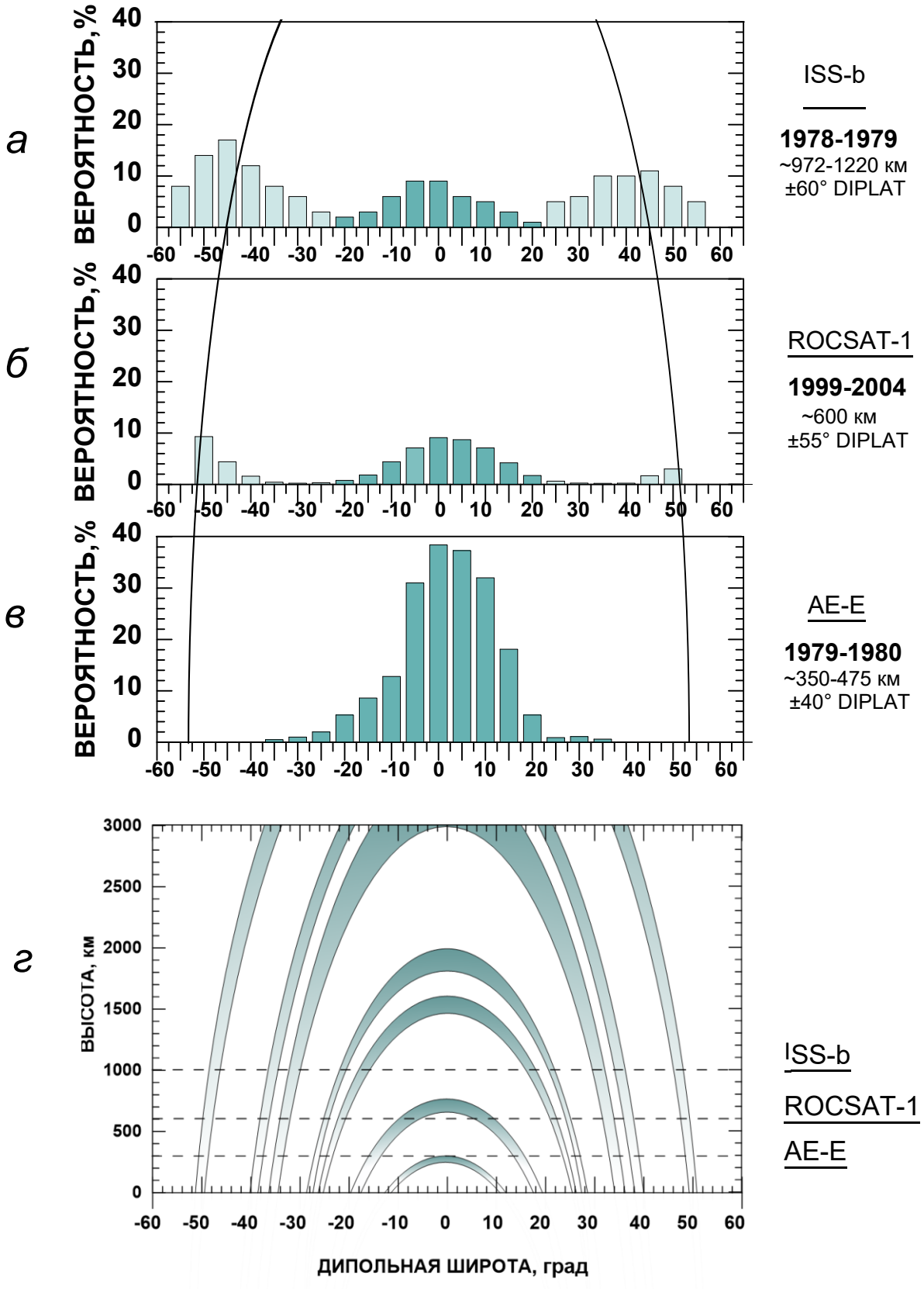
а
б
в
г
ВЕРОЯТНОСТЬ,%
ВЕРОЯТНОСТЬ,%
ВЕРОЯТНОСТЬ,%
ВЫСОТА, км
ДИПОЛЬНАЯ ШИРОТА, град
ISS-b
1978-1979
~972-1220 км
±60° DIPLAT
ROCSAT-1
1999-2004
~600 км
±55° DIPLAT
AE-E
1979-1980
~350-475 км
±40° DIPLAT
ISS-b
ROCSAT-1
AE-E

Fig. 1.

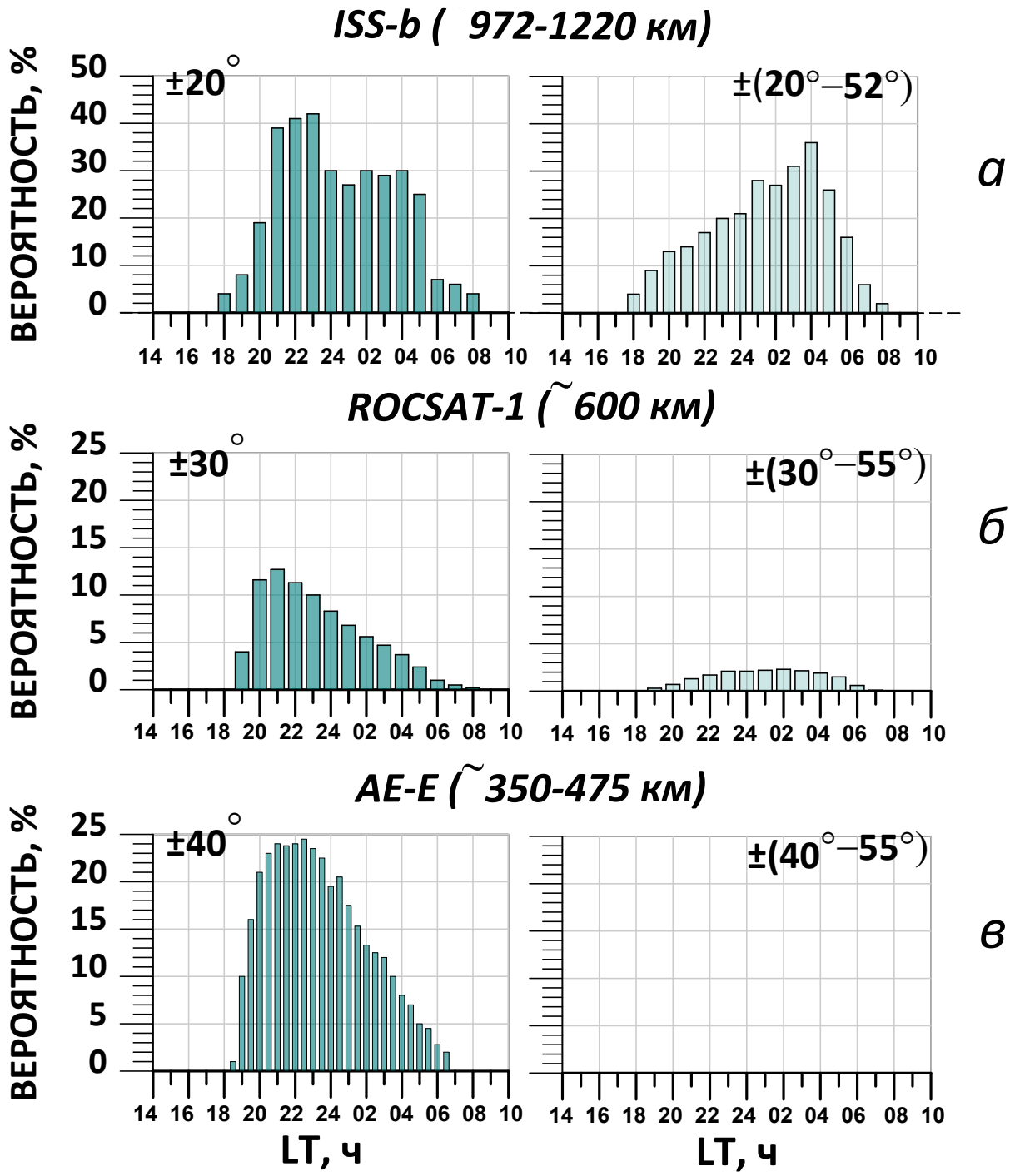
ISS-b (972-1220 км)
ВЕРОЯТНОСТЬ, %
±20°
±(20°–52°)
а
ROCSAT-1 (~600 км)
±30°
±(30°–55°)
б
AE-E (~350-475 км)
±40°
±(40°–55°)
в
LT, ч
LT, ч

Fig. 2.